LRRC52 regulates BK channel function and localization in mouse cochlear inner hair cells

Christopher J. Lingle[a,1,2], Pedro L. Martinez-Espinosa[a,1], Aizhen Yang-Hood[b], Luis E. Boero[b,c], Shelby Payne[b], Dora Persic[d], Babak V-Ghaffari[b], Maolei Xiao[b], Yu Zhou[a], Xiao-Ming Xia[a], Sonja J. Pyott[d], and Mark A. Rutherford[b,2]

[a]Department of Anesthesiology, Washington University School of Medicine, St. Louis, MO 63110; [b]Department of Otolaryngology, Washington University School of Medicine, St. Louis, MO 63110; [c]Instituto de Investigaciones en Ingeniería Genética y Biología Molecular "Dr. Héctor N. Torres," Consejo Nacional de Investigaciones Científicas y Técnicas, 1428 Buenos Aires, Argentina; and [d]Department of Otorhinolaryngology, University Medical Center Groningen, University of Groningen, 9700 RB, Groningen, The Netherlands

Edited by Richard W. Aldrich, The University of Texas at Austin, Austin, TX, and approved July 29, 2019 (received for review April 24, 2019)

The perception of sound relies on sensory hair cells in the cochlea that convert the mechanical energy of sound into release of glutamate onto postsynaptic auditory nerve fibers. The hair cell receptor potential regulates the strength of synaptic transmission and is shaped by a variety of voltage-dependent conductances. Among these conductances, the Ca^{2+}- and voltage-activated large conductance Ca^{2+}-activated K^+ channel (BK) current is prominent, and in mammalian inner hair cells (IHCs) displays unusual properties. First, BK currents activate at unprecedentedly negative membrane potentials (−60 mV) even in the absence of intracellular Ca^{2+} elevations. Second, BK channels are positioned in clusters away from the voltage-dependent Ca^{2+} channels that mediate glutamate release from IHCs. Here, we test the contributions of two recently identified leucine-rich-repeat–containing (LRRC) regulatory γ subunits, LRRC26 and LRRC52, to BK channel function and localization in mouse IHCs. Whereas BK currents and channel localization were unaltered in IHCs from *Lrrc26* knockout (KO) mice, BK current activation was shifted more than +200 mV in IHCs from *Lrrc52* KO mice. Furthermore, the absence of LRRC52 disrupted BK channel localization in the IHCs. Given that heterologous coexpression of LRRC52 with BK α subunits shifts BK current gating about −90 mV, to account for the profound change in BK activation range caused by removal of LRRC52, we suggest that additional factors may help define the IHC BK gating range. LRRC52, through stabilization of a macromolecular complex, may help retain some other components essential both for activation of BK currents at negative membrane potentials and for appropriate BK channel positioning.

BK channels | auxiliary subunits | inner hair cells | LRRC52 | gamma subunits

Sensory hair cells in the cochlea form the cellular gateway that mediates the initial detection of sound. The mechanical energy of sound bends stereocilia positioned at the apical end of the hair cells leading to depolarizing current through mechanoelectrical transduction channels (MET) channels. This MET current generates a receptor potential that depolarizes the hair cells and subsequently activates voltage-dependent Ca^{2+} channels (Cav) at the basolateral end of the hair cell, evoking release of glutamate onto postsynaptic auditory nerve fibers. The hair cell receptor potential and the strength of evoked synaptic transmission elicited by a sound stimulus are also influenced by voltage-dependent conductances intrinsic to hair cells (1, 2). Of these, the Ca^{2+}- and voltage-activated BK current has been of long-standing interest (3–5) because its large amplitude and rapid activation make it well suited to rapidly and robustly shape the receptor potential. Two features of BK currents in mammalian inner hair cells (IHCs) have been of particular interest and remain poorly understood. First, BK currents activate at unprecedentedly negative membrane potentials (−60 mV) even in the absence of intracellular Ca^{2+} elevations (5). Second, BK channels are positioned in clusters away from voltage-dependent Ca^{2+} channels that mediate neurotransmitter release from IHCs, suggesting that voltage-dependent Ca^{2+} influx per se does not participate in BK activation. The molecular determinants that contribute to the unusual activation range of BK channels in IHCs and to clustering and localization remain unknown. Here, we test the contributions of two recently identified leucine-rich-repeat–containing (LRRC) regulatory γ subunits, LRRC26 (γ1) and LRRC52 (γ2) (6), to BK function and localization in mouse IHCs.

Hair cells exhibit a polarized architecture in which the hallmark hair cell mechanotransduction apparatus is positioned apically while neurotransmitter release from the hair cells occurs at the basally positioned ribbon synapses (Fig. 1*A*). In mammalian IHCs, BK channels are clustered away from synapses above the nucleus (7), while the Cav channels required to evoke transmitter release from hair cells are positioned at the basal end near the ribbon synapses. This separation renders BK channels relatively insensitive to Ca^{2+} influx elicited by brief, physiological depolarizations (5). The rapid and robust BK current activation in IHCs is thought to depend on intrinsic properties of the BK channels (5), although contributions of cytosolic Ca^{2+} stores have also been proposed (4). In IHCs, BK channels even at nominally 0 cytosolic Ca^{2+} are appreciably activated at voltages beginning near −60 mV (5), more negative than any BK channel yet described. A useful measure of the range of activation of a

Significance

Hair cells of the cochlea transduce mechanical energy into electrical signals. Acoustic stimulation of mechanotransduction channels generates a graded receptor potential that elicits glutamate release from hair cells onto postsynaptic auditory nerve fibers. The amplitude and time course of the receptor potential is shaped by activation of Ca^{2+}- and voltage-dependent K^+ channels (BK channels). Hair cell BK channels are unusual in that, even in the absence of Ca^{2+}, they are activated at more negative potentials than any other known BK channel. Here we show that a specific regulatory gamma subunit, LRRC52, is a key determinant in inner hair cells of the negative activation range of BK channels. Furthermore, the absence of LRRC52 disrupts BK channel clustering and localization.

Author contributions: C.J.L., S.J.P., and M.A.R. designed research; P.L.M.-E., A.Y.-H., L.E.B., S.P., D.P., M.X., Y.Z., S.J.P., and M.A.R. performed research; X.-M.X. contributed new reagents/analytic tools; C.J.L., B.V.-G., S.J.P., and M.A.R. analyzed data; and C.J.L., S.J.P., and M.A.R. wrote the paper.

The authors declare no conflict of interest.

This article is a PNAS Direct Submission.

[1]C.J.L. and P.L.M.-E. contributed equally to this work.

[2]To whom correspondence may be addressed. Email: clingle@morpheus.wustl.edu or rutherfordmark@wustl.edu.

This article contains supporting information online at www.pnas.org/lookup/suppl/doi:10.1073/pnas.1907065116/-/DCSupplemental.

Published online August 26, 2019.

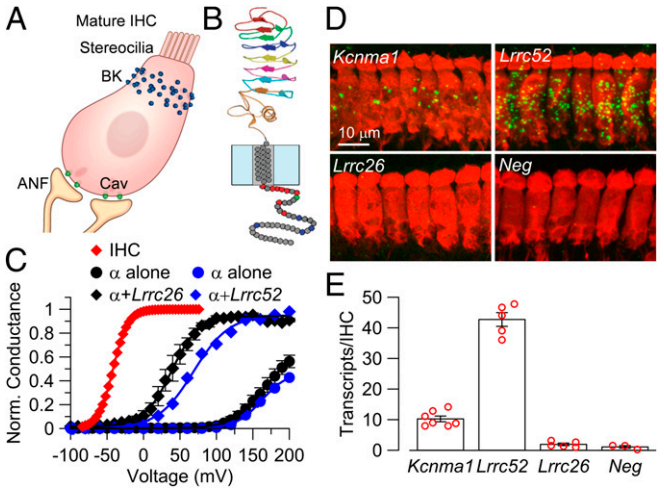

Fig. 1. BK channel regulation by γ subunits and key role of LRRC52 in IHCs. (*A*) Schematic of IHC highlighting mechanosensory transduction apparatus, loci of BK channels, loci of voltage-dependent Ca^{2+} (Cav) channels, and postsynaptic auditory nerve fibers (ANF). Reprinted from ref. 3. Copyright (2016), with permission from Elsevier. (*B*) Transmembrane topology of a γ subunit, based on hagfish lymphocyte receptor homolog (6, 28). Reprinted from ref. 9. (*C*) G-V curves at 0 cytosolic Ca^{2+} were generated from excised inside-out patches from oocytes expressing BK channels with and without the LRRC26(γ1) subunit (black symbols) and with and without the LRRC52(γ2) subunit (blue symbols) (*SI Appendix*, Fig. S2) along with the G-V curve previously reported for whole-cell BK currents in IHCs (red symbols) (5, 28). V_h (summarized in *SI Appendix*, Fig. S1*B*) values were, for IHCs, −41.8 mV; for BK without and with LRRC26, 166.0 ± 1.0 mV (best fit and c.l. [90% confidence limits]) and 38.3 ± 0.6 mV, respectively; and for BK without and with LRRC52, 162.1 ± 1.45 mV and 68.4 ± 2.2 mV, respectively. (*D*) RNAscope images of IHCs in organ of Corti whole-mount showing message for *Kcnma1* (*Top Left*) and *Lrrc52* (*Top Right*), lack of message for *Lrrc26* (*Bottom Left*), and a negative control (*Bottom Right*). Red, calretinin. Green, RNA probe. (*E*) Quantification of detected message from sections as in *D*. Red symbols correspond to average transcripts/IHC from a single field of view of multiple IHCs from a single ear. Adjusted *P* values from ANOVA followed by Tukey's test: *Kcnma1* vs. *Lrrc52*, $P < 0.0001$; *Kcnma1* vs. *Lrrc26*, $P = 0.0011$; *Lrrc52* vs. *Lrrc26*, $P < 0.0001$; *Lrrc52* vs. negative, $P < 0.0001$; *Lrrc26* vs. negative, $P = 0.98$; and *Kcnma1* vs. negative, $P = 0.002$.

voltage-dependent ion channel is its voltage-of-half activation (V_h), the membrane potential at which the channel population is, on average, half open and half closed. The previously reported V_h for rodent IHC BK current, about −40 mV (5), is shifted by ∼210 mV, relative to V_h for BK channels lacking any regulatory subunit at 0 $[Ca^{2+}]_i$ [V_h ∼ +170 mV (8)] (*SI Appendix*, Fig. S1). The basis for this very hyperpolarized gating range of IHC BK current has been a long-standing conundrum, ever since the initial description of a fast gating voltage-dependent K^+ current, termed $I_{K,f}$ (1), now recognized as arising from BK channels (5, 7).

Particular BK regulatory subunits might underlie some of the unusual features of IHC BK current. Of the two known families of BK regulatory subunits, β and γ (9), only γ subunits produce large shifts in BK current activation range at 0 cytosolic Ca^{2+}. Here we focus on two members of the γ subunit family, LRRC26 (γ1) and LRRC52 (γ2). The results show that, whereas BK currents and channel localization were unaltered in IHCs from *Lrrc26* knockout (KO) mice, BK current activation was shifted more than +200 mV in IHCs from *Lrrc52* KO mice. Furthermore, BK channel localization was disrupted in the absence of LRRC52. The profound change in IHC BK channel gating range caused by removal of LRRC52 is much greater than the 90 mV shift observed from heterologous coexpression of LRRC52 with the pore-forming BK channel α subunits. Therefore, we suggest that LRRC52, through the stabilization of a macromolecular complex, may help retain additional components essential for both the activation of BK currents at negative membrane potentials and the appropriate BK channel positioning.

Results

LRRC52 Is Required for Normal IHC BK Channel Function. Regulatory γ subunits of BK channels consist of an extensive extracellular N-terminal LRRC domain, a single transmembrane segment, and a short cytosolic C terminus (Fig. 1*B*) (6, 10). The initial member of this family, LRRC26, produces the largest leftward shift in BK gating of any known BK regulatory subunit, an ∼120- to 130-mV shift in V_h at any $[Ca^{2+}]_i$ (6, 10, 11) and appears largely confined to secretory epithelial cells (12). In secretory epithelial cells expressing endogenous LRRC26-containing BK channels or when LRRC26 is heterologously expressed together with BK α subunits, the V_h of BK activation is about +35 mV at nominally 0 $[Ca^{2+}]_i$ (Fig. 1*C* and *SI Appendix*, Fig. S1) in contrast to the V_h of about +160 to +170 mV for BK channels lacking regulatory subunits. In comparison, LRRC52 produces a somewhat smaller, ∼90- to 100-mV hyperpolarizing shift in the BK current V_h (10) (Fig. 1*C*) over all tested $[Ca^{2+}]_i$ (*SI Appendix*, Fig. S2 *A*–*D*). We also confirmed that both human and mouse forms of LRRC52 produce similar effects (*SI Appendix*, Fig. S2*D*) and that the gating shift produced by LRRC52 is largely stable following patch excision (*SI Appendix*, Fig. S2 *E* and *F*). Despite the known ability of LRRC52 to shift BK gating when coexpressed heterologously, LRRC52 has so far been identified only in mammalian sperm where it is critical to male fertility and where it partners with a different K^+ channel, the Slo3 (*Kcnmu1*) K^+ channel, that underlies the KSPER sperm-specific K^+ conductance (13).

To test whether either LRRC26 or LRRC52 might be present in IHCs, we utilized enhanced in situ hybridization to probe for RNA for *Kcmna1*, *Lrrc52*, and *Lrrc26*. We observed a clear signal for *Kcnma1*, a strong signal for *Lrrc52*, and no signal for *Lrrc26* (Fig. 1*D*). Transcripts per IHC were enriched for *Lrrc52* relative to *Kcnma1*, with *Lrrc26* similar to a negative control (Fig. 1*E*).

We recorded whole-cell currents in IHCs with physiological Na^+ and K^+ gradients, and with pharmacological conditions to isolate BK current (5, 14). IHCs express two major voltage-dependent K^+ currents: first, a rapidly activating current originally termed $I_{K,f}$ and now recognized as arising from BK channels with a threshold near −60 mV and, second, a more slowly activating Kv current, termed $I_{K,s}$, which with brief activation steps begins to be activated only above ∼ −20 mV (1, 5, 15). Here, currents were activated by 5-ms voltage steps from −100 to +40 mV, with tail currents then measured during a subsequent step to −35 mV to determine the relative conductance activated at each test potential (Fig. 2*A*). The 5-ms voltage step is sufficiently brief that most of the current activated arises almost entirely from BK. For IHCs from WT ($IHCs^{WT}$) mice, current begins to be activated near −65 mV with maximal activation of conductance near 0 mV with a V_h for individual cells typically between −35 and −40 mV (Fig. 2*A*). A Boltzmann fit to the averaged conductance-voltage (G-V) curve (Fig. 2*F*) yielded $V_h = -36.5 \pm 0.3$ mV, with $k = 10.3 \pm 0.3$ mV, similar to previous work (5). Confirming this current as BK, IHCs from *Kcnma1* KO ($IHCs^{BK\text{-}KO}$) mice exhibited little outward current activation until around −20 mV, corresponding to the onset of I_{Ks} current (Fig. 1*B*). Furthermore, 200 nM iberiotoxin (IbTx) completely abolished both the tail current relaxations and the steady-state current at −35 mV in WT IHCs (*SI Appendix*, Fig. S3). We then tested whether genetic deletion of either LRRC26 or LRRC52 alters IHC BK current. IHCs from *Lrrc26* KO ($IHCs^{26KO}$) mice exhibited currents essentially indistinguishable from those in $IHCs^{WT}$ (Fig. 2*C*), both in terms of steady-state current density (Fig. 2*E*) and G-V curves (Fig. 2*F*). Remarkably, *Lrrc52* KO resulted in complete loss of detectable BK current (Fig. 2*D*) over

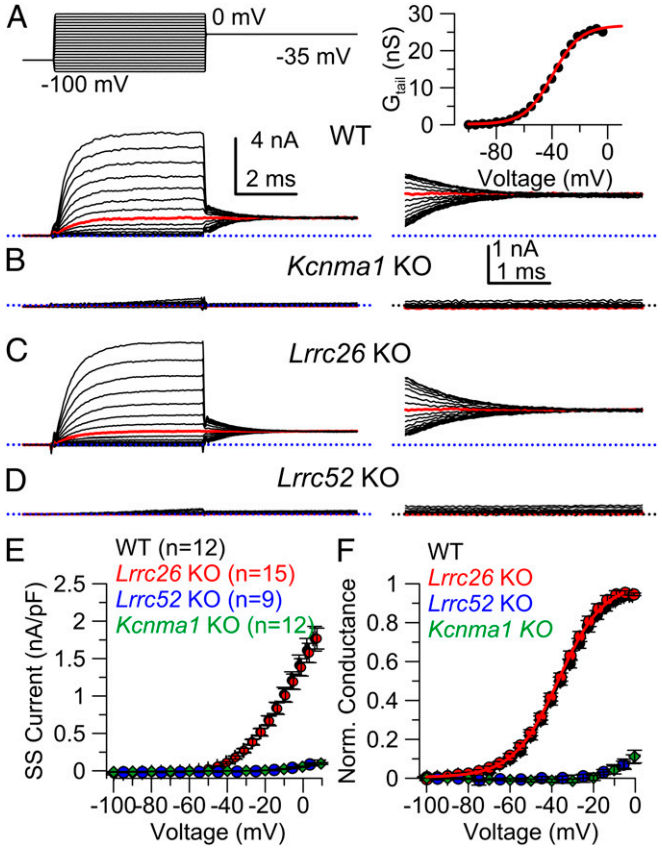

Fig. 2. KO of LRRC52 removes activation of BK current at voltages up to 0 mV. (*A*) Example of BK current from WT IHC and typical stimulation protocol. Red trace, step to −35 mV. (*Right*) Tail currents at −35 mV (at higher gain) used for generation of G-V curve (*Top Right*); $V_h = -38.9 \pm 0.5$ mV; $k = 10.4 \pm 0.5$ mV [0.45 MΩ uncompensated Rs (Rs_{un})]. (*B*) Currents from an $IHC^{BK\text{-}KO}$ activated as in *A*. $I_{K,s}$ current activated during depolarization up to 0 deactivates very slowly at −35 mV and so contributes a small persistent tail current (0.44 MΩ Rs_{un}). (*C*) Sample currents from an IHC^{26KO} (0.68 MΩ Rs_{un}). (*D*) Currents from an IHC^{52KO} (0.27 Rs_{un}). IHCs were obtained from both male (M) and (*F*) female mice of P18 to P35. (*E*) Voltage dependence of outward current from the indicated genotypes and number of cells after normalization to cell capacitance (in pF) and averaging (±SEM). Current densities (at 0 mV) in $IHCs^{WT}$ and $IHCs^{26KO}$ were indistinguishable (ANOVA with Tukey's test: $P = 0.6952$) as was that between $IHCs^{BK\text{-}KO}$ and $IHCs^{52KO}$ ($P > 0.999$). Current densities in both $IHCs^{BK\text{-}KO}$ and $IHCs^{52KO}$ (at 0 mV) differed from those in $IHCs^{WT}$ and $IHCs^{26KO}$ (WT vs. BK-KO, $P < 0.0001$; WT vs. 52KO, $P < 0.0001$; 26KO vs. BK-KO, $P \leq 0.0001$; 26KO vs. 52KO, $P < 0.0001$). Note that symbols in *E* and *F* for WT and 26KO largely overlap, while BK-KO and 52KO also overlap. (*F*) G-V curves were normalized to the fitted peak conductance and averaged (±SEM). Parameters (mean ± c.l.) for single Boltzmann fits were, for $IHCs^{WT}$, $V_h = -36.50 \pm 0.29$ mV with $k = 10.35 \pm 0.28$ mV and, for $IHCs^{26KO}$, $V_h = -36.86 \pm 0.40$ mV and $k = 10.76 \pm 0.37$ mV. For WT, mean values from 12 separate IHCs were (±SEM) $V_h = -35.83 \pm 1.04$ mV with $k = 10.90 \pm 0.61$ mV, with average $Rs_{un} = 0.59 \pm 0.06$ MΩ. For *Lrrc26*, mean values from 14 cells were (±SEM) $V_h = -36.37 \pm 1.01$ mV, with $k = 10.75 \pm 0.51$ mV and average $Rs_{un} = 0.57 \pm 0.06$ MΩ. V_h and k values measured for 12 $IHCs^{WT}$ and 14 $IHCs^{26KO}$ were indistinguishable (ANOVA with Tukey's test: for V_h, $P = 0.8691$; for k, $P = 0.9778$).

this voltage range. Both steady-state outward current density and G-V curves from IHCs from *Lrrc52* KO ($IHCs^{52KO}$) mice were indistinguishable from those of $IHC^{BK\text{-}KO}$ (Fig. 2 *E* and *F*). LRRC52 is therefore necessary for activation of BK current over the normal physiological range of membrane potentials in mouse IHCs.

BK Current Is Activated at Positive Voltages in $IHCs^{52KO}$. That LRRC52 is a major molecular determinant of the gating range of BK channels in IHCs seems surprising. On one hand, LRRC52 alone shifts BK gating by only about −95 mV when coexpressed heterologously, whereas the G-V of $IHCs^{WT}$ is shifted about −210 mV relative to BK channels lacking any regulatory subunits. Does LRRC52 alone account for the BK gating range in IHCs? Furthermore, LRRC52 has been previously described as a sperm-specific partner of the *Kcnu1*-encoded Slo3 alkalization-activated K^+ channel (13, 16). Given that many sperm ion channels, ion exchangers, and proteins are thought to be sperm-specific (17–20), the presence of LRRC52 in loci other than sperm was unexpected. We therefore wondered whether any BK current was present in $IHCs^{52KO}$. To test this, we measured BK activation using voltage steps up through +200 (or +220) mV with tail currents measured at +40 mV (Fig. 3). Such protocols are not useful in $IHCs^{WT}$, because of large BK current densities at voltages positive to +40 mV. The more positive tail current

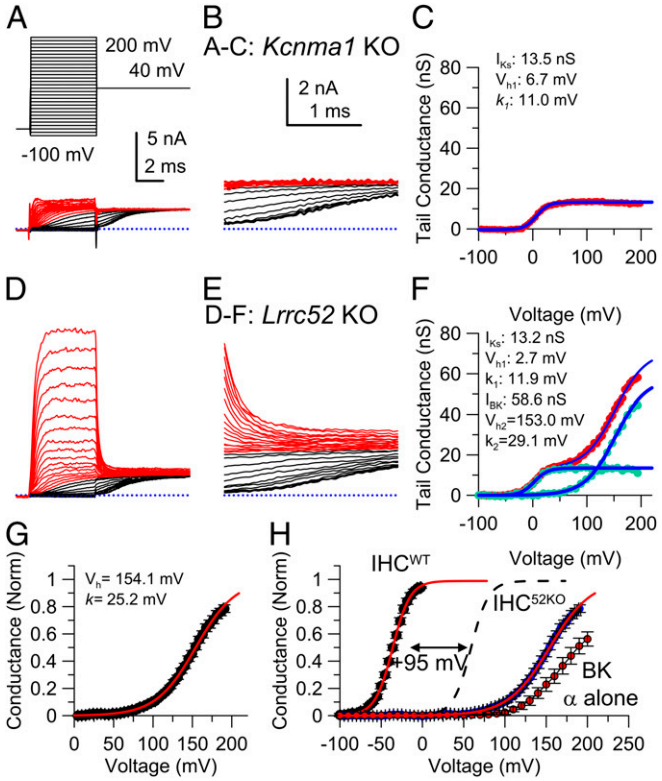

Fig. 3. IHCs from *Lrcc52* KO mice express functional BK currents that activate positive to +100 mV. (*A*) Voltage steps to +200 mV were used to activate current in an IHC from a *Kcnma1* KO mouse. (*B*) Tail currents following repolarization to +40 mV (beginning 150 μs following nominal voltage step) are shown for the cell in *A* with black traces corresponding to depolarizing steps from −100 mV through +35 mV, while red corresponds to traces from +40 to +200 mV. (*C*) G-V curve generated from tail current at 150 μs following repolarization to +40 mV with a best-fit single Boltzmann curve (blue curve) overlaying the data points ($V_h = 6.7 \pm 0.6$ mV; $k = 11.0 \pm 0.5$ mV). This corresponds to fractional activation of I_{Ks} current following 5 ms at indicated voltages. (*D*) Activation of outward current as in *A*, but for *Lrrc52* KO. (*E*) Tail currents at +40 mV for the cell in *D*. (*F*) G-V curve (red symbols) generated from tail current from the cells in *D* and *E*, with an overlaid best fit of a two-component Boltzmann ($A_1 = 13.2 \pm 0.5$ nS, $V_{h1} = 2.7 \pm 1.6$ mV, $k_1 = 11.9 \pm 1.2$ mV, $A_2 = 58.6 \pm 1.5$ ns, $V_{h2} = 153.0 \pm 1.2$ mV, $k_2 = 29.1 \pm 1.2$ mV). Green symbols are the two components of conductance, isolated via subtraction of each fit component (overlaid blue lines) from the original G-V curve. (*G*) Averaged G-Vs for individual normalized (to G_{max} of Boltzmann fit) G-Vs for each $IHCs^{52KO}$ are shown along with best fit (red line: $V_h = 154.2 \pm 0.7$ mV, $k = 25.2 \pm 0.3$ mV). (*H*) Comparison of IHC^{WT} BK G-V (Fig. 2*F*), BK α G-V at 0 Ca^{2+} (from Fig. 1*C*), high-voltage–activated conductance in $IHCs^{52KO}$ (*G*), and the $IHCs^{WT}$ BK G-V shifted by +95 mV (dashed line).

potential is required because rapid deactivation of BK current lacking regulatory subunits precludes meaningful estimation of relative conductances (*SI Appendix*, Fig. S4 *A* and *B*). We reasoned that comparisons between $IHCs^{BK\text{-}KO}$ and $IHCs^{52KO}$ using very positive depolarizations might reveal the onset of BK current activation in $IHCs^{52KO}$, but not in $IHCs^{BK\text{-}KO}$. In $IHCs^{BK\text{-}KO}$, steps up to +200 mV activated voltage-dependent outward current, which exhibited little increase in amplitude from +40 up to +200 mV (Fig. 3*A*). Activation steps from +40 to +200 mV result in essentially identical tail currents measured at +40 mV (Fig. 3 *A* and *B*, red traces). For steps up to +40 mV, the tails reflect the partial activation of I_{Ks} during the 5-ms voltage step (black traces), and there is no additional activation of I_{Ks} above +40 mV (red traces). Measurement of tail currents at +40 mV following steps from −100 to +220 mV resulted in a G-V curve well described by a single Boltzmann function reflecting the voltage dependence of activation of a single component of conductance, presumably I_{Ks} (Fig. 3*C*). Thus, in $IHCs^{BK\text{-}KO}$, there is no additional activation of any voltage-dependent conductance above +40 mV.

When the same protocol is applied to $IHCs^{52KO}$, the outward current increases appreciably up through +200 mV (Fig. 3*D*), with tail currents exhibiting an additional component of current deactivation following voltage steps above +100 mV (Fig. 3*E* and *SI Appendix*, Fig. S4 *D–F*). The tail current G-V contains both a component of conductance similar to that observed in $IHCs^{BK\text{-}KO}$ (Fig. 3*C*), likely arising from $I_{K,s}$, and a second component that does not attain full saturating activation even at +220 mV (Fig. 3*F*). Such G-V curves could be well fit by a two-component Boltzmann with one component of conductance essentially identical to that in $IHCs^{BK\text{-}KO}$ and a second component with a V_h around +150 to +155 mV (Fig. 3*F*). For a set of 11 $IHCs^{52KO}$, individual G-Vs share a similar range of activation for the higher voltage component with a fit to the averaged G-Vs yielding a maximum conductance of 59.7 ± 0.7 nS with $V_h = 150.3 \pm 0.7$ mV and $k = 23.9 \pm 0.4$ mV. A fit to the averaged, normalized G-Vs yielded a $V_h = 154.1 \pm 0.7$ mV with $k = 25.2 \pm 0.2$ mV (Fig. 3*G*). The symmetric nature of the Boltzmann distribution provides confidence that the fit estimates are a reasonable description of the conductance observed at positive voltages, despite the absence of a saturating current level in the G-Vs.

In sum, the $IHCs^{52KO}$ express a current activated at potentials positive to +100 mV that is absent in $IHCs^{BK\text{-}KO}$, while the properties of the Kv conductance activated negative to +100 mV were indistinguishable between $IHCs^{BK\text{-}KO}$ (*SI Appendix*, Fig. S5*A*) and $IHCs^{52KO}$ (*SI Appendix*, Fig. S5*B*). Current densities and activation range of IbTx-resistant current measured in $IHCs^{WT}$ treated with 200 nM IbTx were also similar (*SI Appendix*, Fig. S5*C*) to that in the $IHCs^{BK\text{-}KO}$ and $IHCs^{52KO}$. Overlay of the normalized G-Vs for these three conditions (*SI Appendix*, Fig. S5*D*) highlights that the slowly activating Kv current present in the $IHCs^{WT}$, $IHCs^{BK\text{-}KO}$, and $IHCs^{52KO}$ was essentially identical in each case. Thus, the absence or alteration of BK current properties in $IHCs^{BK\text{-}KO}$ and $IHCs^{52KO}$ does not seem to result in any compensatory change in current density or current properties of the residual Kv currents observed in $IHCs^{WT}$. It should be noted that the absolute magnitudes of these current densities are almost certainly reduced by inclusion of 4-AP in our solutions, but this reduction should be similar in all three genotypes.

The extra conductance activated at higher voltages in $IHCs^{52KO}$ shares properties with that of BK current arising from *Kcnma1* α subunits expressed alone in heterologous systems (Fig. 3*H*), including a similar V_h (~ +154 mV vs. ~ +160 to 165 mV) and a characteristic reduced voltage dependence for activation at 0 Ca^{2+}. If the loss of LRRC52 was simply shifting BK gating by the +95-mV shift observed when LRRC52 and BK α subunits are coexpressed, the expected V_h would be about +55 mV (dashed line in Fig. 3*H*). We undertook two tests to further confirm that the extra conductance in $IHCs^{52KO}$ is, in fact, BK current. First, we compared tail currents following activation with depolarizations up to +220 mV with tail currents at either −35 mV (*SI Appendix*, Fig. S4 *A–C*) or +40 mV (*SI Appendix*, Fig. S4 *D–F*). This comparison revealed that, at −35 mV, the currents activated at positive potentials deactivated so rapidly as to be barely detectable at 150 μs following repolarization (*SI Appendix*, Fig. S4*B*), in contrast to the robust tails observed at +40 mV (*SI Appendix*, Fig. S4*E*). Furthermore, the extra conductance in $IHCs^{52KO}$ was inhibited by IbTX (*SI Appendix*, Fig. S4 *D–H*). Together, these results indicate that BK currents are still expressed in $IHCs^{52KO}$ and that the absence of LRRC52 results in an ~210-mV shift in the BK activation range, much larger than the 95-mV effect exerted by LRRC52 acting alone on BK channels (*SI Appendix*, Fig. S2). This raises the possibility that some other factor/component is lost from the BK channels following *Lrrc52* KO.

Do any other known BK regulatory subunits participate in the gating shift? Although this question is beyond the scope of the present paper, a few comments are appropriate. The BK γ3 (LRRC55) subunit is unlikely to participate since by itself it produces only a minor effect on BK gating (10) and it obviously does not substitute for LRRC52 following in the LRRC52 KO. Previous work excluded both β1 and β4 subunits as participants in defining IHC BK channel properties (21, 22), but β2 and β3 subunits have not been evaluated. When LRRC26 and β2 subunits coassemble in the same BK channel, their effects on gating are largely additive (23). The β2 subunits produce no gating shift at 0 cytosolic Ca^{2+} (23) and so would not be expected to contribute in IHCs. However, we measured BK current in IHCs from mice lacking the β2 (*Kcnmb2*) subunit (*SI Appendix*, Fig. S6) and found that they are indistinguishable from currents in WT IHCs. The β3 (*Kcnmb3*) KO mice are not yet available. Although deserving future attention, any shift arising from β3 seems unlikely to participate in the 210-mV shift observed when LRRC52 is removed. Overall, based on properties (9, 24) of known β and γ subunits, it is unlikely that the very negative range of BK gating in IHCs arises from some combination of BK β and γ regulatory subunits with LRRC52 subunits.

BK Clustering and Localization Are Disrupted in $IHCs^{52KO}$. We next examined immunofluorescent localization of BK channel distribution on IHCs from WT and KO mice. In $IHCs^{WT}$, BK channels are organized in ~10 to 20 clusters per IHC (Fig. 4 *A* and *E*) ranging in size from 0.22 to 5.1 μm with a mean long axis per cluster of 1.58 ± 0.94 μm ($n = 97$ clusters on 7 midcochlear IHCs). BK immunoreactivity was completely absent in $IHCs^{BK\text{-}KO}$ (Fig. 4*B*), while BK channel localization in $IHCs^{26KO}$ was similar to $IHCs^{WT}$ (Fig. 4*C*). In contrast, in $IHCs^{52KO}$, BK channels are diffusely distributed over the entire plasma membrane extending from the apical plate to the basolateral ribbon synapses (Fig. 4 *D–F*). The tendency of BK channels to be intensely clustered on the neck region of $IHCs^{WT}$ (Fig. 4*E*) appears entirely absent in $IHCs^{52KO}$ (Fig. 4*F*). Thus, the absence of LRRC52 causes not only a rightward shift in the activation curve of BK currents but also a loss of BK channel clustering and localization.

$IHCs^{52KO}$ and $IHCs^{BK\text{-}KO}$ Respond Similarly to Injected Current. Given the role of BK channels in shaping the IHC receptor potential and, thereby, the response properties of the postsynaptic auditory nerve fibers (25), we measured membrane potential responses to 100-ms steps of injected current in IHCs from mice of different genotypes. Voltage responses to square wave current injection exhibit an initial transient depolarization reflecting a combination of any depolarizing conductances, the time course of K^+ current activation, and cell charging time. In $IHCs^{WT}$, following a small, transient depolarization, each injected current leads to a steady-state depolarization that increases modestly with injected current (Fig. 5*A*). In $IHCs^{BK\text{-}KO}$, similar current injection results in larger and more slowly decaying transient depolarization that reaches a steady-state level ~9 mV more

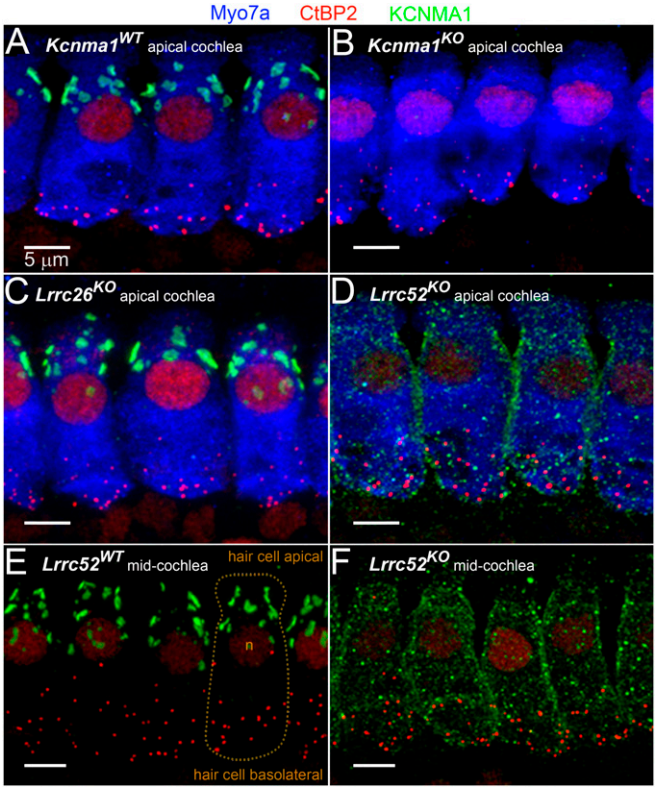

Fig. 4. *Lrrc52* KO, but not *Lrrc26* KO, disrupts localization of BK channel immunoreactivity. (*A*) Organ of Corti whole-mount immunolabeling of BK channels (KCNMA1, green) at apical end of IHC in dense clusters below stereocilia and above nuclei in a WT mouse (P30). Blue, myosin 7a, a cytoplasmic marker. Red, CtBP2, a marker of the presynaptic ribbons and nuclei. (Scale bar for all panels: 5 μm.) (*B*) Image from apical cochlea in *Kcnma1* KO, showing lack of BK immunoreactivity. (*C*) Image from *Lrrc26* KO, showing clustered localization as in WT. (*D*) Image from *Lrrc52* KO, showing mislocalization of KCNMA1 subunits throughout the membrane. (*A*–*D*) Image was taken from the 9-kHz tonotopic location. (*E*) Labeling for BK and CtBP2 in the absence of Myo7a Ab to allow better visualization of BK labeling in a P30 WT mouse. Dotted line outlines a single IHC. (*F*) As in *E*, but with P30 *Lrrc52* KO mouse. (*E* and *F*) Midcochlea (37 kHz) location. (*A*–*F*) Maximum-intensity projections.

depolarized than in IHCs^{WT} (Fig. 5*B*). In IHCs^{52KO}, depolarizations in response to current injection are essentially indistinguishable from those in IHCs$^{BK\text{-}KO}$ (Fig. 5*C*). The properties of the transient depolarization in both IHCs$^{BK\text{-}KO}$ and IHCs^{52KO} are consistent with the absence of the rapidly activating BK current, which normally serves to shunt the effects of depolarizing current injection. The relationship between injected current and peak depolarization (Fig. 5*D*) shows no significant difference between IHCs$^{BK\text{-}KO}$ and IHCs^{52KO}, with both being clearly different from IHCs^{WT}. For steady-state voltages, the differences between WT and either of the KO strains are significant over all current injection amplitudes (Fig. 5 legend), although small in absolute terms compared to the differences seen for peak depolarizations. The more negative steady-state membrane potential in IHCs^{WT} presumably arises because of the contributions of both some persistent BK along with the slowly activating $I_{K,s}$. The similarity of peak depolarization in both IHCs^{52KO} and IHCs$^{BK\text{-}KO}$ (Fig. 5*D*) indicates that, despite the presence of BK current in the IHCs^{52KO}, the shifted range of activation of that current renders it unable to dampen IHC depolarization, which in vivo is mediated by MET currents (25). Although auditory deficits in BK KO mice are subtle, we predict that any auditory deficits arising from IHCs would be essentially identical between *Lrrc52* and *Kcnma1* KO mice.

Discussion

Here we demonstrate that LRRC52 is a critical determinant of the unusually negative gating range of BK channels in mouse IHCs and that the absence of LRRC52 disrupts the localization and clustering of BK channels in IHCs. That LRRC52, but not LRRC26, plays this role is somewhat surprising since LRRC52 was previously described as a sperm-specific regulatory subunit of the Slo3 K^+ channel in mouse sperm (13, 16) and also because LRRC26 shifts BK gating more than LRRC52. The present results establish clearly that LRRC52 is a regulatory partner of two distinct channel gene products, KCNMA1/Slo1 (BK) and KCNU1/Slo3, each with distinct physiological roles, but both depending on LRRC52 to define normal physiological functions.

An unexplained aspect of the results is that KO of LRRC52 abolishes, perhaps completely, the gating shift of BK channels in IHCs^{WT}. Whereas LRRC52 can shift BK gating about −90 mV when partnered in heterologous expression systems, the absence of LRRC52 in IHCs shifts BK gating by ∼210 mV. Thus, the effects of LRRC52 alone on BK gating seem insufficient to account for the BK gating range in IHCs^{WT}. How is this to be explained? The observation that *Lrrc52* KO also disrupts BK localization and clustering suggests the possibility that loss of LRRC52 results in dissolution of part or all of a BK macromolecular complex, which may contain other elements that contribute to the full 210-mV gating shift. Disruption of BK localization in the *Lrrc52* KO is similar to the idea that LRRC52 plays a critical role in linking together a complex of molecular components that define BK function and localization. Although proteomic identification of BK-associated proteins in cochlea has failed to identify either LRRC52 or other obvious BK regulatory components (26), comparison of BK-associated proteins between WT and *Lrrc52* KO mice may shed light on this issue. Whatever the basis for the large gating shift in the absence of LRRC52, any additional component that may contribute to the shift requires the presence of LRRC52 either to be effective or to be part of the BK complex.

Given the prominence of BK current in IHCs, there has been considerable interest in its role in auditory function (15, 25), but many of the effects of BK absence are subtle. Neither auditory brainstem responses (ABR) nor distortion product otoacoustic emissions reveal clear differences in the excitability threshold for hearing of low-level sounds (7, 22), although ABR wave 1 amplitude may be reduced suggesting reduced spike synchrony in auditory nerve fibers of the *Kcnma1* KO (27). In recordings from single auditory nerve fibers, latencies of action potential firing are increased and maximum firing rates reduced in BK KO mice (25). Furthermore, BK KO mice may exhibit accelerated age-related hearing loss (22). In noise-induced hearing loss, BK KO mice may have increased temporary threshold shifts, but studies have reported contradictory results on noise-induced permanent threshold shifts (21, 27). Given the similar response to injected current in both IHCs^{52KO} and IHCs$^{BK\text{-}KO}$, we would anticipate that any auditory deficits arising from dysfunction of IHC BK currents would be common to both *Lrrc52* and *Kcnma1* KO mice. This may seem somewhat surprising given that BK channels are still present in IHCs^{52KO}, with some channels presumably more closely positioned to voltage-dependent Ca^{2+} channels than in WT mice. Although future tests may reveal conditions under which the residual BK channels in IHCs from *Lrrc52* KO mice are activated under physiological conditions, here we see no indication that influx of Ca^{2+} during 5-ms depolarizations can activate any BK current in IHCs^{52KO}. Furthermore, even during 100-ms current injections, there is no distinction between the voltage behavior of IHCs$^{BK\text{-}KO}$ or IHCs^{52KO}. As such, the absence of LRRC52 in IHCs is likely to fully mimic the effect of complete KO of the BK α subunit. The key role of LRRC52 in defining BK function and localization also raises the possibility that deficits in BK function in native IHCs might arise if there are processes that lead to down-regulation of LRR52 expression.

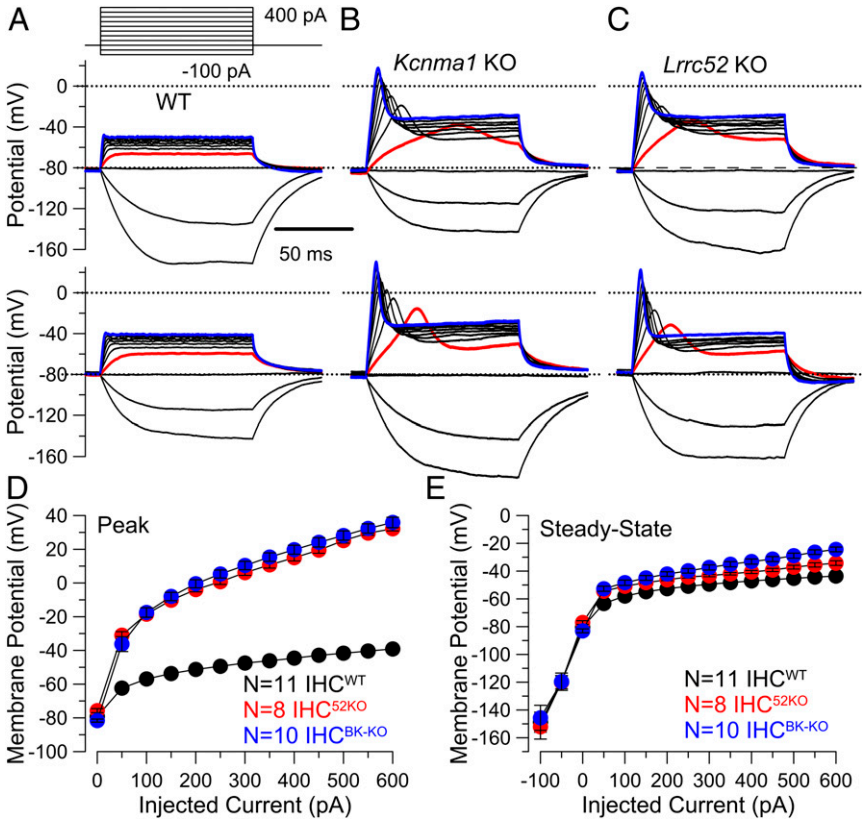

Fig. 5. Voltage responses to injected current are identical in $IHCs^{52KO}$ and $IHCs^{BK-KO}$. Voltage responses to injected constant current pulses (−100 to 400 pA in 50-pA increments) for (*A*) 2 $IHCs^{WT}$, (*B*) 2 $IHCs^{BK-KO}$, and (*C*) 2 $IHCs^{52KO}$. Red and blue traces are responses to +50 pA and +400 pA, respectively. (*D*) Averaged peak voltages (±SEM) for a set of cells from each genotype (WT: $n = 11$; *Lrrc52* KO: $n = 8$; *Kcnma1* KO: $n = 10$). A two-way ANOVA with Tukey's test (*Materials and Methods*) was used to evaluate membrane potential responses among genotypes for current injection from +100 pA through +600 pA. For WT vs. *Lrrc52*, adjusted $P < 0.001$; for WT vs. *Kcnma1* KO, $P < 0.001$; and for *Lrrc52* KO vs. *Kcnma1* KO, $P = 0.5262$. (*E*) Averaged steady-state voltages (±SEM) for each genotype. From two-way ANOVA with Tukey's test (+100 pA through +600 pA), for WT vs. *Lrrc52*, $P < 0.0001$ and for WT vs. *Kcnma1* KO, $P < 0.0001$, while for *Lrrc52* KO vs. *Kcnma1* KO, $P = 0.0899$.

The results here open up an unanticipated aspect of the role of BK channels in IHCs. That LRRC52 KO results in essentially complete loss of the shifted gating of IHC BK current and also disrupts BK clustering and localization draws attention to the idea that the clustering and localization of BK channels are an important part of its biological function in IHCs. Furthermore, to account for the full loss of the 210-mV gating shift in $IHCs^{WT}$ and the loss of BK clustering in the $IHCs^{52KO}$, we have suggested that BK channels, when aggregated together with LRRC52, are also assembled in large macromolecular assemblies with additional regulatory elements. Further work on IHCs and, specifically, BK-containing macromolecular complexes may help identify new regulatory elements that serve to fine-tune BK channel function in ways not yet anticipated.

Materials and Methods

Animals. Animals (mice and *Xenopus*) were handled and housed according to the National Institutes of Health Committee on Laboratory Animal Resources guidelines. All experimental protocols were approved by the Institutional Animal Care and Use Committees of Washington University (protocols #20180288 and #20180125). All mice were C57BL/6, with KO alleles backcrossed out to at least 8 generations. The *Lrrc26* KO mice were as previously described (12) with the neomycin expression cassette present in the original Knockout Mouse Project (KOMP) Repository line deleted (12). The *Lrrc52* KO mice were also described in previous work (16). *Lrrc26* and *Lrrc52* lines of mice are available from the KOMP Repository (https://www.komp.org).

Cochlea Explants and Whole-Cell Recordings from IHCs. Cochlea explants (5, 14, 25) were isolated from postnatal day 18 (P18) to P35 male and female mice in the following dissection solution (in mM) of 144 NaCl, 5.8 KCl, 0.9 $MgCl_2$, 1.3 $CaCl_2$, 0.7 NaH_2PO_4, 10 Hepes, 5.6 D-glucose (pH 7.4 at 306 mOs). For recordings, explants were maintained in a standard physiological solution containing (in mM) 155 NaCl, 5.8 KCl, 0.9 $MgCl_2$, 1.3 $CaCl_2$, 0.7 NaH_2PO_4, 10 Hepes, 5.6 D-glucose, with 1 μM XE-991 to inhibit KCNQ current and 5 mM 4-AP to reduce I_{Ks} (pH 7.4 at 320 mOs). The pipette solution contained (in mM) 150 KCl, 3.5 $MgCl_2$, 0.1 $CaCl_2$, 5 EGTA, 2.5 Na_2ATP, 5 Hepes, with 15 mM 4-AP to reduce I_{Ks} (pH 7.4 at 312 mOs). Gigaseals were formed on visually identified IHCs with pipettes of 1.5 to 2 MΩ resistance. Slight suction was utilized to achieve the whole-cell configuration. Experiments were at nominal room temperature (22 to 25 °C.). Additional methods are provided in *SI Appendix*.

ACKNOWLEDGMENTS. This work was initially supported by a Center for Investigation of Membrane Excitability Diseases pilot project (M.A.R. and C.J.L.), and also supported in part by NIH Grants R35GM118114 and NS100695 (C.J.L.). The work was also supported by the Washington University Department of Anesthesiology (C.J.L.), by a University of Groningen Rosalind Franklin Fellowship (S.J.P.), by the Washington University Department of Otolaryngology (M.A.R.), and by National Institute of Deafness and Other Communication Disorders Grant R01DC014712 (M.A.R.). We thank Joe Henry Steinbach for discussions regarding statistical methods.

1. C. J. Kros, A. C. Crawford, Potassium currents in inner hair cells isolated from the Guinea-pig cochlea. *J. Physiol.* **421**, 263–291 (1990).
2. R. J. Helyer, H. J. Kennedy, D. Davies, M. C. Holley, C. J. Kros, Development of outward potassium currents in inner and outer hair cells from the embryonic mouse cochlea. *Audiol. Neurotol.* **10**, 22–34 (2005).
3. S. J. Pyott, R. K. Duncan, BK channels in the vertebrate inner ear. *Int. Rev. Neurobiol.* **128**, 369–399 (2016).
4. W. Marcotti, S. L. Johnson, C. J. Kros, Effects of intracellular stores and extracellular Ca(2+) on Ca(2+)-activated K(+) currents in mature mouse inner hair cells. *J. Physiol.* **557**, 613–633 (2004).

5. H. Thurm, B. Fakler, D. Oliver, Ca^{2+}-independent activation of BKCa channels at negative potentials in mammalian inner hair cells. *J. Physiol.* **569**, 137–151 (2005).
6. J. Yan, R. W. Aldrich, LRRC26 auxiliary protein allows BK channel activation at resting voltage without calcium. *Nature* **466**, 513–516 (2010).
7. S. J. Pyott, E. Glowatzki, J. S. Trimmer, R. W. Aldrich, Extrasynaptic localization of inactivating calcium-activated potassium channels in mouse inner hair cells. *J. Neurosci.* **24**, 9469–9474 (2004).
8. F. T. Horrigan, R. W. Aldrich, Coupling between voltage sensor activation, Ca^{2+} binding and channel opening in large conductance (BK) potassium channels. *J. Gen. Physiol.* **120**, 267–305 (2002).
9. V. Gonzalez-Perez, C. J. Lingle, Regulation of BK channels by beta and gamma subunits. *Annu. Rev. Physiol.* **81**, 113–137 (2019).
10. J. Yan, R. W. Aldrich, BK potassium channel modulation by leucine-rich repeat-containing proteins. *Proc. Natl. Acad. Sci. U.S.A.* **109**, 7917–7922 (2012).
11. V. Gonzalez-Perez, X. M. Xia, C. J. Lingle, Functional regulation of BK potassium channels by γ1 auxiliary subunits. *Proc. Natl. Acad. Sci. U.S.A.* **111**, 4868–4873 (2014).
12. C. Yang *et al*., Knockout of the LRRC26 subunit reveals a primary role of LRRC26-containing BK channels in secretory epithelial cells. *Proc. Natl. Acad. Sci. U.S.A.* **114**, E3739–E3747 (2017).
13. C. Yang, X. H. Zeng, Y. Zhou, X. M. Xia, C. J. Lingle, LRRC52 (leucine-rich-repeat-containing protein 52), a testis-specific auxiliary subunit of the alkalization-activated Slo3 channel. *Proc. Natl. Acad. Sci. U.S.A.* **108**, 19419–19424 (2011).
14. D. Oliver, M. Knipper, C. Derst, B. Fakler, Resting potential and submembrane calcium concentration of inner hair cells in the isolated mouse cochlea are set by KCNQ-type potassium channels. *J. Neurosci.* **23**, 2141–2149 (2003).
15. C. J. Kros, J. P. Ruppersberg, A. Rüsch, Expression of a potassium current in inner hair cells during development of hearing in mice. *Nature* **394**, 281–284 (1998).
16. X. H. Zeng, C. Yang, X. M. Xia, M. Liu, C. J. Lingle, SLO3 auxiliary subunit LRRC52 controls gating of sperm KSPER currents and is critical for normal fertility. *Proc. Natl. Acad. Sci. U.S.A.* **112**, 2599–2604 (2015).
17. M. A. Nolan *et al*., Sperm-specific protein kinase A catalytic subunit Calpha2 orchestrates cAMP signaling for male fertility. *Proc. Natl. Acad. Sci. U.S.A.* **101**, 13483–13488 (2004).
18. P. Ramaraj, S. P. Kessler, C. Colmenares, G. C. Sen, Selective restoration of male fertility in mice lacking angiotensin-converting enzymes by sperm-specific expression of the testicular isozyme. *J. Clin. Invest.* **102**, 371–378 (1998).
19. C. M. Santi *et al*., The SLO3 sperm-specific potassium channel plays a vital role in male fertility. *FEBS Lett.* **584**, 1041–1046 (2010).
20. D. Wang, S. M. King, T. A. Quill, L. K. Doolittle, D. L. Garbers, A new sperm-specific Na^+/H^+ exchanger required for sperm motility and fertility. *Nat. Cell Biol.* **5**, 1117–1122 (2003).
21. S. J. Pyott *et al*., Cochlear function in mice lacking the BK channel alpha, beta1, or beta4 subunits. *J. Biol. Chem.* **282**, 3312–3324 (2007).
22. L. Rüttiger *et al*., Deletion of the Ca2+-activated potassium (BK) alpha-subunit but not the BKbeta1-subunit leads to progressive hearing loss. *Proc. Natl. Acad. Sci. U.S.A.* **101**, 12922–12927 (2004).
23. V. Gonzalez-Perez, X. M. Xia, C. J. Lingle, Two classes of regulatory subunits coassemble in the same BK channel and independently regulate gating. *Nat. Commun.* **6**, 8341 (2015).
24. X. Zeng, X. M. Xia, C. J. Lingle, Species-specific differences among KCNMB3 BK beta3 auxiliary subunits: Some beta3 N-terminal variants may be primate-specific subunits. *J. Gen. Physiol.* **132**, 115–129 (2008).
25. D. Oliver *et al*., The role of BKCa channels in electrical signal encoding in the mammalian auditory periphery. *J. Neurosci.* **26**, 6181–6189 (2006).
26. T. Kathiresan, M. Harvey, S. Orchard, Y. Sakai, B. Sokolowski, A protein interaction network for the large conductance Ca(2+)-activated K(+) channel in the mouse cochlea. *Mol. Cell. Proteomics* **8**, 1972–1987 (2009).
27. S. F. Maison, S. J. Pyott, A. L. Meredith, M. C. Liberman, Olivocochlear suppression of outer hair cells in vivo: Evidence for combined action of BK and SK2 channels throughout the cochlea. *J. Neurophysiol.* **109**, 1525–1534 (2013).
28. H. M. Kim *et al*., Structural diversity of the hagfish variable lymphocyte receptors. *J. Biol. Chem.* **282**, 6726–6732 (2007).